

Multi-wavelength analysis of the SN-associated low-luminosity GRB 171205A

LI, XIU-JUAN,^{1,2} ZHANG, ZHI-BIN[†],¹ HUANG, YONG-FENG,^{3,4,5} AND XU, FAN³

¹*School of Physics and Physical Engineering, Qufu Normal University, Qufu 273165, China, z_b_zhang@sina.com*

²*School of Cyber Science and Engineering, Qufu Normal University, Qufu 273165, China, lxj@qfnu.edu.cn*

³*School of Astronomy and Space Science, Nanjing University, Nanjing 210023, China*

⁴*Key Laboratory of Modern Astronomy and Astrophysics (Nanjing University), Ministry of Education, Nanjing 210023, China*

⁵*Xinjiang Astronomical Observatory, Chinese Academy of Sciences, 150 Science 1-Street, Urumqi 830011, China*

(Received , 2023; Revised , 2023; Accepted , 2023)

Submitted to ApJ

ABSTRACT

Multi-wavelength properties of the nearby Supernova(SN)-associated low-luminosity GRB 171205A are investigated in depth to constrain its physical origin synthetically. The pulse width is found to be correlated with energy with a power-law index of -0.24 ± 0.07 , which is consistent with the indices of other SN/GRBs but larger than those of long GRBs. By analyzing the overall light curve of its prompt gamma-rays and X-ray plateaus simultaneously, we infer that the early X-rays together with the gamma-rays should reflect the activities of central engine while the late X-rays may be dominated by the interaction of external shocks with circumburst material. In addition, we find that the host radio flux and offset of GRB 171205A are similar to those of other nearby low-luminosity GRBs. We adopt 9 SN/GRBs with measured offset to build a relation between peak luminosity ($L_{\gamma,p}$) and spectral lag (τ) as $L_{\gamma,p} \propto \tau^{-1.91 \pm 0.33}$. The peak luminosity and the projected physical offset of both 12 SN/GRBs and 10 KN/GRBs are found to be moderately correlated, suggesting their different progenitors. The multi-wavelength afterglow fitted with a top-hat jet model indicates that the jet half-opening angle and the viewing angle of GRB 171205A are ~ 34.4 and 41.8 degrees, respectively, which implies that the off-axis emissions are dominated by the peripheral cocoon rather than the jet core.

Keywords: High energy astrophysics (739); Gamma-ray bursts (629);

1. INTRODUCTION

Gamma-ray bursts (GRBs) are the most energetic gamma-ray flashes in the universe. They are consisted of two stages: an initial prompt gamma-ray emission phase and a long-lasting multi-wavelength afterglow emission phase (Zhang & Mészáros 2004; Zhang 2007; Kumar & Zhang 2015; Zhang 2018). Physically, the prompt emissions are considered to originate from internal shocks due to the interactions between ejected materials inside the fireball, while the broadband afterglows are produced by external shocks due to ejecta-medium interactions (e.g. Mészáros & Rees Meszaros1997; Sari 1997; Huang et al. 2000; Zhang 2018). In general, the collapsar model is thought to account for long GRBs (LGRBs) with a duration of $T_{90} > 2$ s (Paczynski 1998; Woosley & Heger 2006). So far, a handful of LGRBs are observed to be associated with energetic, broad-lined, stripped-envelope supernovae (SNe). These

SN-associated GRBs usually have a luminosity 3 \sim 4 orders of magnitude lower than normal LGRBs (e.g. Galama et al. 1998; Pian et al. 2006).

The light curves of prompt emissions are variable and highly irregular, reflecting the temporal properties of the internal energy dissipation and the activities of the central engine (e.g. Rees & Meszaros 1994; Li et al. 2020). Besides, the spectral properties of GRBs contain the key information of radiative mechanisms (Norris et al. 1996). For example, the time lags of light curve between different energy bands can be used to understand the emission mechanism of prompt emissions (Zhang et al. 2006a; Wei et al. 2017). Generally, when the higher energy photons arrive earlier than lower energy photons, we call it a positive time lag. Otherwise, it is called a negative lag. Norris et al. (2000) reported an anti-correlation between the peak luminosity ($L_{\gamma,p}$) and the time lag (τ) for six BATSE LGRBs, which can be described by a power-law function as

$L_{\gamma,p} \propto \tau^{-1.14}$. At the same time, they found that the SN-associated GRB 980425 falls below the extrapolated power-law function by a factor of 400 – 700. Subsequently, the anti-correlation between $L_{\gamma,p}$ and τ was further investigated and confirmed with different samples (e.g. Norris 2002; Schaefer & Collazzi 2007; Hakkila et al. 2008; Arimoto et al. 2010; Ukwatta et al. 2010, 2012; Bernardini et al. 2015). However, whether the $L_{\gamma,p} - \tau$ relation exists for the SN/GRBs is unknown yet until Li et al. (2023) recently built the luminosity relation $L_{\gamma,p} \propto \tau^{-1.43 \pm 0.33}$ by using of 16 Supernova-associated GRBs (SN/GRBs). In addition, they also utilized 14 kilonova-associated GRBs (KN/GRBs) to build a power-law relation of $L_{\gamma,p} \propto \tau^{-2.17 \pm 0.57}$.

Two leading types of central engines, i.e., (1) a hyper-accreting black hole (BH) and (2) a rapidly spinning, strongly magnetized neutron star (NS), have been proposed to power the GRB outflows (e.g. Usov 1992; Popham et al. 1999; Zhang & Mészáros 2001). Long-lasting emissions of GRBs in the forms of extended emissions and X-ray afterglows, are crucial to reveal the physical origin of the central engines (Zhang et al. 2006; Norris & Bonnell 2006; Rowlinson et al. 2013; Lü et al. 2015, 2018, 2020; Kisaka et al. 2017; Sharma et al. 2021). Based on the dipole spin-down model, Lü et al. (2015) confirmed the hypothesis of the magnetar central engine model for short GRBs (SGRBs) with an “internal plateau” followed by a very rapid decay. In view of the energetics of GRBs, the central engines of LGRBs with energies larger than 10^{52} erg are preferentially identified as black holes (Sharma et al. 2021). Nevertheless, the unusual observations of low-luminosity GRBs (LLGRBs) suggest some different emission processes, such as a less-collimated outflow, a choked jet, or even spherical ejecta moving at mildly relativistic speeds (Nakar & Sari 2012; Bromberg et al. 2011). Their intrinsic features such as energetics, temperatures, and timescales are explained very well by shock breakout emissions (Kulkarni et al. 1998; Nakar & Sari 2012; Izzo et al. 2019).

Several nearby LLGRBs such as GRB 980425/SN 1998bw, GRB 031203/SN 2003lw, GRB 060218/SN 2006aj, GRB 100316D/SN 2010bh, GRB 171205A/SN 2017iuk, GRB 190829A/SN 2019oyu, are identified to be associated with SNe (e.g. Galama et al. 1998; Malesani et al. 2004; Starling et al. 2011; Pian et al. 2006; Campana et al. 2006; Terreran et al. 2019). A systematic study of the time lags in the prompt emissions of both the SN/GRBs and KN/GRBs (Li et al. 2023) and the similarity between SN/GRB 171205A and KN/GRB 170817A motivate us to undertake further analysis in more detail. In fact, the properties of

GRB 171205A were found to be different from other energetic GRBs and other LLGRBs in many respects (e.g. D’Elia et al. 2018; Wang et al. 2018; Izzo et al. 2019; Zhang et al. 2022). Therefore, it is necessary for us to go further to compare this burst with other nearby LLGRBs systematically in this study. This paper is organized as follows. Data analysis and methods are given in Section 2. The main results are presented in Section 3. Finally, the discussion and conclusions are presented in Section 4 and Section 5, respectively.

2. OBSERVATIONS AND DATA PREPARATION

2.1. Basic properties

On 2017 December 5 at 07:20:43.9 UT, the Swift Burst Alert Telescope (Swift/BAT) triggered and located GRB 171205A (D’Elia et al. 2017), whose duration is long as $T_{90} = 190.5 \pm 33.9$ s as measured from $T - 26.2$ to $T + 164.3$ s (Izzo et al. 2017) and the time-averaged spectrum is best fit by a power-law function with a photon index of $\alpha_{\text{PL}} = -1.99_{-0.82}^{+0.59}$ while the fluence and the peak photon flux in the 15 - 350 keV band are $6.78_{-0.89}^{+0.99} \times 10^{-6}$ erg cm^{-2} and $1.02_{-0.29}^{+0.29}$ ph cm^{-2} s^{-1} (Lien et al. 2016). The afterglow observations of GRB 171205A were carried out in multiple wavelengths from X-rays to radio bands up to 1000 days (e.g. Kennea et al. 2017; Butler et al. 2017; Izzo et al. 2017; Cobb 2017; Choi et al. 2017; Chandra et al. 2017a,b; D’Elia et al. 2018; Urata et al. 2019; Leung et al. 2021; Maity & Chandra 2021). Spectroscopic observations revealed that GRB 171205A is associated with a Type Ic SN 2017iuk (Izzo et al. 2017; Wang et al. 2018; D’Elia et al. 2018). It is also found that GRB 171205A occurred in the outskirts of the bright spiral galaxy 2MASX J11093966-1235116 locating at $z = 0.037$, which is an early-type (S0), high-mass, star-forming galaxy with a low specific star formation rate and a low metallicity (Izzo et al. 2017; Wang et al. 2018). Throughout this study, a flat Λ CDM Universe with $\Omega_m = 0.286$, $\Omega_\Lambda = 0.714$ and $H_0 = 69.6$ km s^{-1} Mpc^{-1} is assumed (Bennett et al. 2014).

2.2. Data analysis

To study the relation between luminosity and spectral lag for GRB 171205A, we first compare three different kinds of lags including the cross correlation function (CCF) lag τ (Band 1997), the centroid delay τ_c and the peak time delay τ_p (Norris et al. 2000) between channel 1 (15-25 keV), channel 2 (25-50 keV), channel 3 (50-100 keV) and channel 4 (100-350 keV). It proves that the CCF method can provide the best lags with relatively smaller scatter (see Figure 2 for a detail). Consequently, the CCF lag will be calculated and applied

for all GRBs in our sample herein. The mask-weighted light-curve data with a 10 s resolution are taken from the Swift website ¹ (Lien et al. 2016). We take two steps to obtain the more accurate spectral lags. First, in order to obtain the smooth CCF curves, we follow Zhang et al. (2006a,b, 2008) to fit the light-curve data using the “KRL” function of individual GRB pulse and obtain four smooth light curve pulses (Li et al. 2020, 2021a, 2022a). Then, we perform the CCF analysis with the Stingray PYTHON package (Huppenkothen et al. 2019a,b) ².

Two distinct components could be observed following the prompt emission of many GRBs. One is a high-level extended emission and the other is a low-level plateau stage. Kisaka et al. (2017) used a phenomenological formula to depict these two components, which essentially synthesizes two functions (each has a constant flux stage followed by a subsequent power-law decay). Considering that the two power-law indexes could be different for the two components, we modify their empirical formula as

$$L_{X,\text{iso}}(t) = L_{\text{EX,iso}}(1 + \frac{t}{T_{\text{EX}}})^{\alpha_1} + L_{\text{PL,iso}}(1 + \frac{t}{T_{\text{PL}}})^{\alpha_2}, \quad (1)$$

where $L_{\text{EX,iso}}$, $L_{\text{PL,iso}}$, T_{EX} , and T_{PL} are the luminosities and durations of the extended and plateau emissions, and α_1 and α_2 are the temporal indexes, respectively. Note that the extended emission as emission with a timescale of $\lesssim 10^3$ s, some of which are not detected by Swift/BAT. A longer timescale component ($\gtrsim 10^3$ s) is defined as plateau emission (Kisaka et al. 2017). The identification of the extended and plateau emission is purely phenomenological (Kisaka et al. 2017).

3. RESULTS

3.1. Dependence of Pulse Width on Energy

We now examine the dependence of the full width at half maximum (FWHM) on the averaged photon energy (E). The FWHM versus photon energy is plot in Figure 1. Here the errors of FWHM are estimated by considering the error propagation, using the method proposed in our previous study (Zhang et al. 2006a). Considering the fact that a larger bin size of light curve can improve the signal-to-noise level but also can smooth the pulse structures (Li et al. 2021a), we here use the observed light curves with a time resolution of 10s. It is feasible since GRB 171205A is a very long burst and it can be divided into sufficient bin numbers to ensure its essential temporal profiles.

¹ <https://swift.gsfc.nasa.gov/results/batgrbcats>

² <https://docs.stingray.science/core.html>

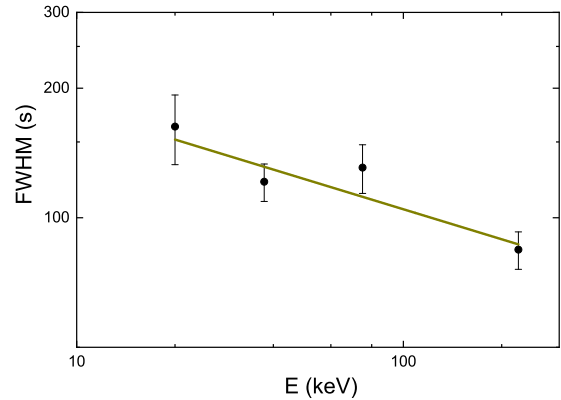


Figure 1. The FWHM and the averaged photon energy of GRB 171205A in the four energy channels are anti-correlated. The solid line stands for the best power-law fit to the data.

It could be seen that the negative power-law correlation, $FWHM \sim E^\alpha$, still holds for GRB 171205A, with a Pearson coefficient of $\rho = 0.92$ and a chance probability of $P = 0.08$. Our best fit power-law index is $\alpha = -0.24 \pm 0.07$, which is coincident with those observed in GRB 980425 ($\alpha = -0.20 \pm 0.04$) and GRB 060218 ($\alpha = -0.31 \pm 0.03$) (Liang et al. 2006; Zhang 2008), but is significantly larger than the value of -0.4 for normal LGRBs (Fenimore et al. 1995; Norris et al. 1996). In addition, we find that the power-law index of GRB 171205A is marginally consistent with the mean value of $\alpha = -0.32 \pm 0.03$ for single-peaked BATSE SGRBs (Li et al. 2020) and $\alpha = -0.32 \pm 0.02$ for Swift SGRBs (Li et al. 2021a). Physically, the energy-dependent burst duration is related to the evolution of peak energy across the observing band (Campana et al. 2006; Uhm et al. 2018). Considering the fact that most KN/GRBs are short in duration, one can conclude that SN /GRB 171205A shares the partial properties of KN/GRBs, which has also been illustrated on the plane of luminosity versus spectral lag (Li et al. 2023). The overlapping features of SN- and KN-GRBs add more complexity to the GRB classification. The best solution is to assort GRBs with more physical parameters jointly (e.g. Zhang et al. 2009).

3.2. Peak Luminosity versus Time Lag

To check whether GRB 171205A matches the $L_{\gamma,p} - \tau$ relation, one needs to precisely measure the time lags of light curves across different energy channels. The CCF lag was adopted more frequent than either the peak lag or the centroid lag since these basic techniques were proposed in the past (Band 1997; Norris et al. 2000).

Three types of lags between distinct energy channels in diverse time resolutions are compared for GRB 171205A in Figure 2, where it can be found that the CCF lags with a bin size of 10 s have relatively smaller errors and the centroid lags are larger than the others. Therefore, the CCF lag τ_{31} between energy channels 1 and 3 is chosen to compare GRB 171205A with other SN/GRBs and KN/GRBs in the plot of $L_{\gamma,p}$ versus τ_{31} . The three types of lags are listed in Table 1.

Figure 3 is plotted to examine whether SN/GRBs and KN/GRBs with known offsets in our sample obey the power-law relations of $L_{\gamma,p} \propto \tau_{31}^{\zeta}$, in which $L_{\gamma,p}$ is calculated with $L_{\gamma,p} = 4\pi D_L^2 P_{\gamma, \text{bolo}}$. Here D_L is the luminosity distance, $P_{\gamma, \text{bolo}} = P_{\gamma} K_c$ is the bolometric peak flux, and K_c is the K-correction factor (Zhang et al. 2018a, 2020). The lags have been corrected by the factor $(1+z)^{-1}$ to compensate for the cosmological time dilation. The spectral lag is proportional to the pulse width with a factor of $(1+z)$ for the cosmological time dilation and a factor of $(1+z)^{-0.33}$ for the frequency shift (Li et al. 2020, 2021a). As a result, the ratio of the intrinsic time lag to the observed one is $(1+z)^{-0.67}$ (see also Gehrels et al. 2006). The errors of lag are calculated by considering the error propagation process as done in our previous study (Zhang et al. 2006a). We find that the lags of the SN/GRBs are longer than those of the KN/GRBs, which can be understood if the time lags are related to the burst durations through the emission radius and Lorentz factor (Zhang et al. 2009). In particular, we find the new luminosity relation is

$$\log L_{\gamma,p} = (49.62 \pm 0.35) - (1.91 \pm 0.33) \log \tau_{31}, \quad (2)$$

with a Pearson coefficient of $\rho = 0.91$ and a chance probability of $P = 7.11 \times 10^{-4}$ for the SN/GRBs, which is consistent with those based on a large sample of SN/KN-connected GRBs (Li et al. 2023) but differ from the one given by Norris et al. (2000) for six normal LGRBs. For the KN/GRBs, it can be seen that most lags are nearly zero, which is very close to previous results for short GRBs (e.g. Norris & Bonnell 2006; Zhang et al. 2006b; Bernardini et al. 2015). However, it is hard to obtain a firm conclusion due to the limited sample of KN/GRBs with measured offset. In addition, we caution that GRB 171205A exhibits a time lag close to the averaged one of normal LGRBs (see e.g. Norris et al. 2000; Zhang et al. 2006a,b) and it lies near the fitting line of SN/GRBs, which further strengthens its association with a supernova.

Since most bright GRBs are found to have narrower pulses and smaller lags (Band 1997; Norris et al. 2000), it is straightforward to expect the power-law relation between luminosity and spectral lag as shown in Eq.

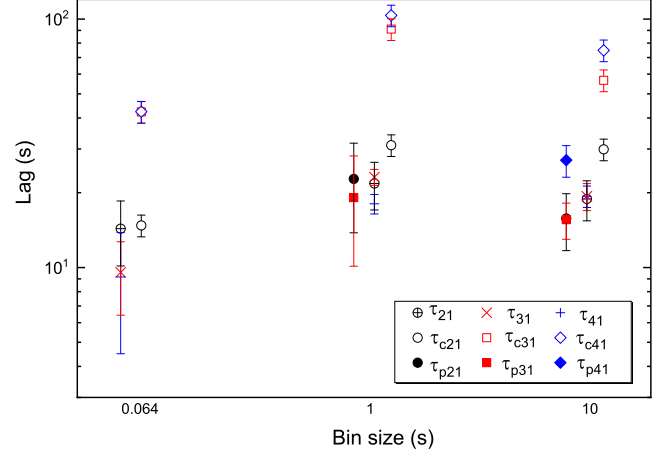


Figure 2. The CCF lags (crosses), the peak lags (filled symbols) and the centroid lags (empty symbols) measured between different energy channels in time bins of 64 ms, 1 s and 10 s, respectively.

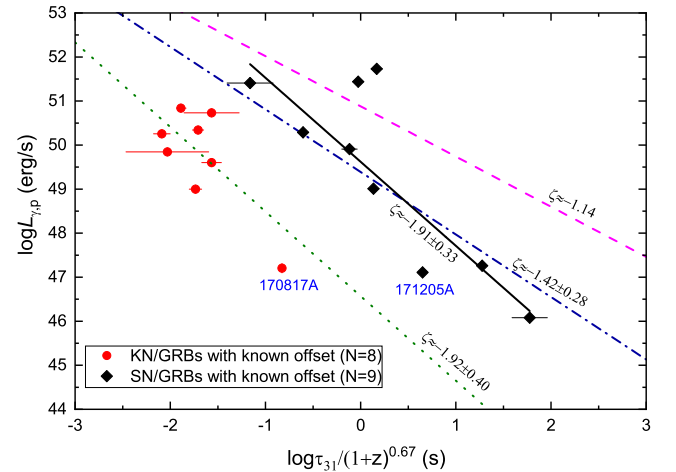


Figure 3. The best fitting results of the $L_{\gamma,p} - \tau_{31}$ relations for 9 SN/GRBs (solid line) with measured offsets in this work, for 16 SN/GRBs (dash-dotted line) and 14 KN/GRBs (dotted line) with known redshifts in Li et al. (2023). The $L_{\gamma,p} - \tau_{31}$ relation built with 7 LGRBs unassociated with SNe (Norris et al. 2000) is also shown by the dashed line.

(2). Because short GRBs have zero lags due to very fast variability (Zhang et al. 2006b), the luminosity-lag/time correlation could be insignificant among them, while the power-law relation is quite significant for long GRBs (Norris et al. 2000; Zhang et al. 2006a).

3.3. Extended Emission and Plateau Emission

Table 1. The detailed values of lags under different bin sizes.

Bin size	τ_{p21}^a	τ_{p31}^a	τ_{p41}^a	τ_{c21}^b	τ_{c31}^b	τ_{c41}^b	τ_{21}^c	τ_{31}^c	τ_{41}^c
0.064 s	-- ^d	-- ^d	-- ^d	14.77±1.48	42.31±4.23	42.37±4.24	9.16±4.66	9.56±3.13	14.33±4.19
1 s	22.72±8.93	19.12±9.00	-- ^d	31.09±3.11	91.10±9.11	103.40±10.34	18.05±1.62	23.12±1.70	21.78±4.73
10 s	15.76±4.06	15.58±2.59	27.02±3.93	29.89±2.99	56.68±5.67	74.81±7.48	19.69±1.91	19.36±2.41	18.88±3.46

Note:

a– the peak lags.

b– the centroid lags. We calculate the centroid as $t_{\text{centroid}} = \sum I(t)t\Delta t / \sum I(t)\Delta t$, where Δt is the time bin of the observed data and $I(t)$ is the pulse intensity (Zhang 2008). Note that the inferred errors of the centroid lags are large and we just take 10% of the centroid lags as an error estimation in our calculations.

c– the CCF lags.

d– the signal in the corresponding bin size is too weak to be well fitted by a pulse function.

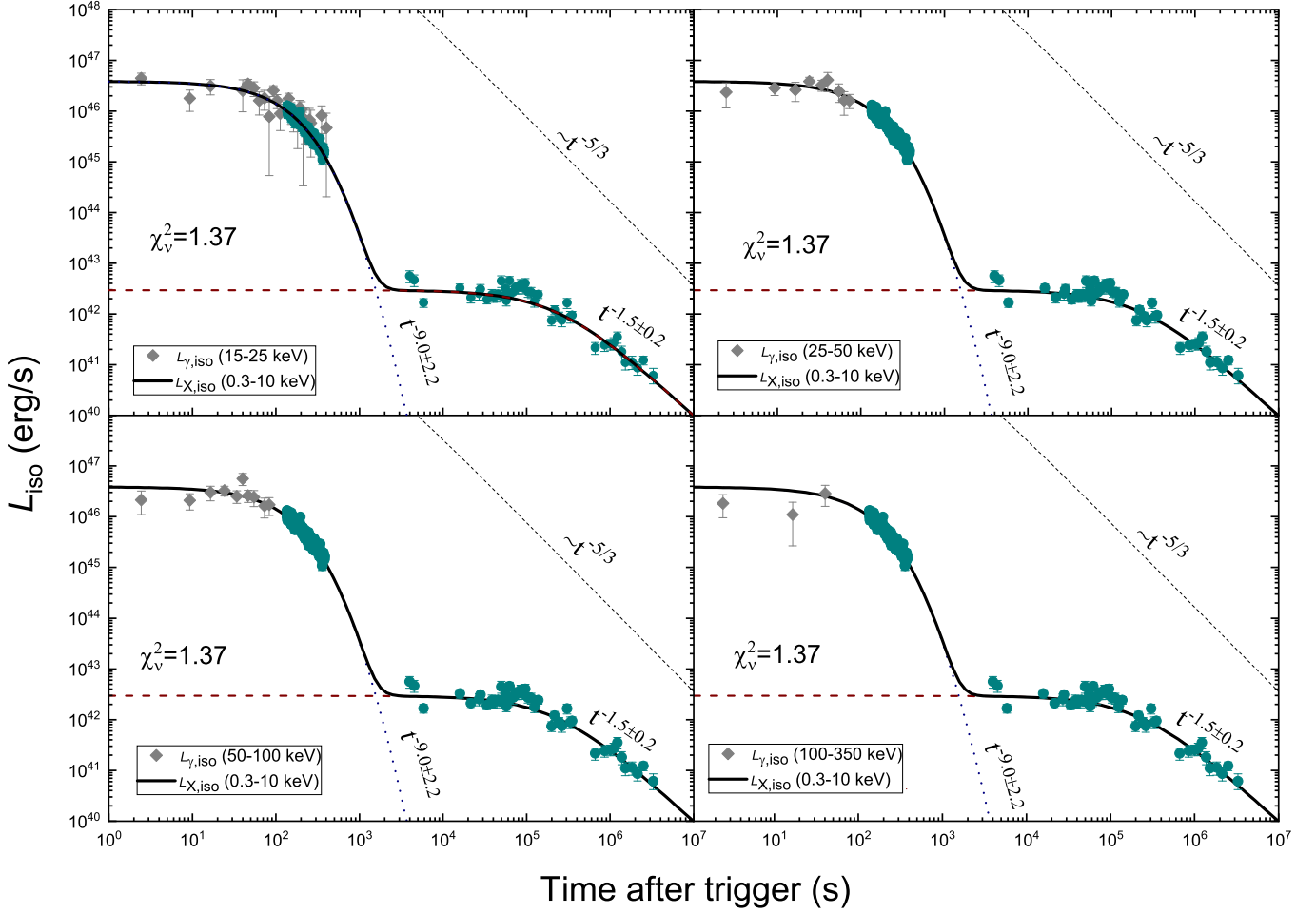


Figure 4. The joint light curves of the prompt multi-wave band γ -ray emissions (gray diamonds) and the X-ray emissions (green circles) of GRB 171205A. Note that the data points in BAT bands are chosen with high SNR ($\text{SNR} \geq 2$). The solid line stands for the best fit to the XRT data with Equation (1). The dotted lines show the total luminosity of the Blandford-Znajek (BZ) jet launched by an evolving BH with a power-law timing index of $\alpha = -5/3$ (Rosswog 2007; Kisaka & Ioka 2015; Kisaka et al. 2017).

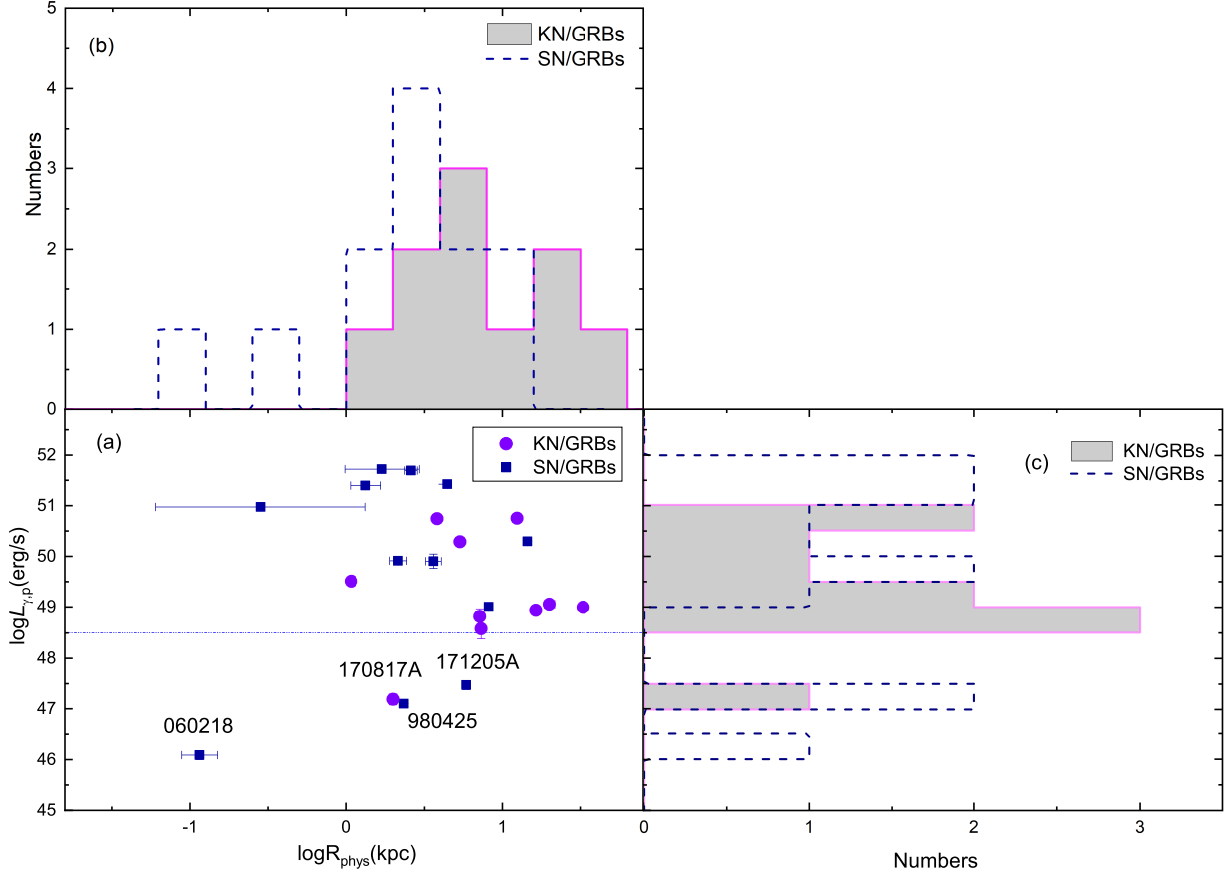


Figure 5. One-dimensional (Panels b and c) and two-dimensional (Panel a) $L_{\gamma,p} - R_{\text{phys}}$ distributions of 12 SN/GRBs and 10 KN/GRBs. In Panel a, the long horizontal line corresponds to the upper limit of $L_{\gamma,\text{iso}} \sim 10^{48.5} \text{ erg s}^{-1}$ for LLGRBs derived by Cano et al. (2017).

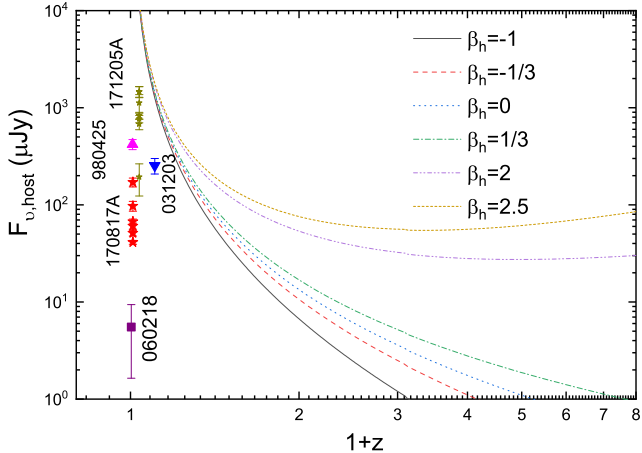


Figure 6. Radio flux densities of GRB host galaxies versus their redshifts. The lines correspond to different spectrum indexes of $\beta_h = -1$ (solid), $-1/3$ (dashed), 0 (dotted), $1/3$ (dash-dotted), 2 (dot-dot-dashed), and 2.5 (short dashed) in Zhang et al. (2018b). The $F_{\nu, \text{host}}$ values of GRBs 060218, 980425, and 031203 are also taken from Zhang et al. (2018b). The $F_{\nu, \text{host}}$ values of GRBs 171205A (yellow circle) and 170817A (red star) are estimated in this study, at the frequencies of 3.5 GHz and 7.1 GHz, respectively.

By jointly analyzing both the Swift/BAT³ and XRT⁴ data, we now investigate the potential connection between the extended emission and the plateau component. The X-ray luminosity of GRB 171205A can be calculated as $L_{X, \text{iso}} = 4\pi D_L^2 F(1+z)^{-(2-\Gamma)}$ (Tang et al. 2019; Xu et al. 2021), where $\Gamma = 1.63$ is the photon spectral index taken from the Swift GRB table⁵. The prompt γ -ray light curves in the four BAT energy channels and the X-ray plateau emissions of GRB 171205A are presented in Figure 4, where we find that the Swift/BAT light curves in all energy bands perfectly bridge with the XRT afterglow. This indicates that both γ -ray and early X-ray components should reflect the activities of the central engine together and could share the same radiation mechanism.

Furthermore, we perform a temporal fit to the X-ray light curve of GRB 171205A by adopting Equation 1. The best-fit results are $L_{\text{EX}, \text{iso}} = (3.86 \pm 0.11) \times 10^{46}$ erg s⁻¹, $L_{\text{PL}, \text{iso}} = (2.95 \pm 0.24) \times 10^{42}$ erg s⁻¹, $T_{\text{EX}} = (840.03 \pm 241.66)$ s, $T_{\text{PL}} = (2.40 \pm 0.08) \times 10^6$ s, $\alpha_1 = -9.0 \pm 2.2$, and $\alpha_2 = -1.5 \pm 0.2$ with a reduced chi-square of $\chi_\nu^2 \simeq 1.37$ (see Figure 4). The late X-ray plateau followed by a shallower decay could be mainly

contributed by the energy injection from a magnetar (e.g. Zhang & Mészáros 2001; Fan & Xu 2006; Tang et al. 2019), the jet viewed off-axis (Beniamini 2020) or the fall-back accretion process of black hole (BH) (Yu et al. 2015), which reflects the multiple activities of the central engine. Of course, the possibility that the X-ray plateau is contributed by a Supernova SN2017iuk cannot be fully ruled out (D’Elia et al. 2018; Li et al. 2023). Interestingly, GRB 171205A favors a magnetar origin although it has an external plateau in X-rays (Wang et al. 2023). The power-law index of $\alpha_2 = -1.5 \pm 0.2$ of the second decay segment at late time (tens of days after trigger) is very close to the expected value of $(4 - 3p)/2 \sim 1.6$ for an electronic spectral index of $p = 2.4$ in the standard afterglow theory (Gao et al. 2013), which demonstrates that the late-time decay should be dominated by the interaction of external shocks with circumburst material. This does not conflict with the magnetar origin that can be dominant in the early X-ray phase. Very recently, we analyzed those GRBs with internal X-ray plateaus and found that the prompt gamma-ray durations are tightly correlated with the plateau lasting times (Du et al. 2023), which indicates that the early X-ray emissions including plateaus should originate from some internal processes, such as the dissipation of magnetars.

3.4. The host and offset

For standard GRBs and high-luminosity GRBs, Zhang et al. (2018b) found a similar redshift independence of the flux for host galaxies. Only three nearby LLGRBs deviate from the relation. Li et al. (2015) statistically investigated the relation between the host flux density (F_{host}) and the peak afterglow flux density ($F_{\text{o, peak}}$) in radio bands, and derived a useful tight correlation as $F_{\nu, \text{host}} = (b_1 + b_2\nu)F_{\text{o, peak}}$ for LLGRBs, with $b_1 = 0.27 \pm 0.02$ and $b_2 = -0.016 \pm 0.002$, where ν is the observing frequency. Using this correlation, we can estimate the $F_{\nu, \text{host}}$ of GRB 171205A at frequencies with $F_{\text{o, peak}}$ available. Using the radio data provided in Leung et al. (2021) and Maity & Chandra (2021), we have calculated the radio flux density of the host galaxy of GRB 171205A. The result is illustrated in Figure 6 and is compared with several other GRB hosts. It can be seen that the host spectral index ($\beta_h < -1$) of GRB 171205A is significantly less than the average spectral index $\langle \beta_h \rangle \sim -0.75$ of spiral galaxies (Condon 1992), which is similar to other nearby LLGRBs, but differs from the high-luminosity or standard GRBs. In addition, we find that GRB 170817A as a peculiar short GRB associated with both gravitational wave and kilonova is located in the region with a lower spectral index of

³ <https://swift.gsfc.nasa.gov/results/batgrbcats>

⁴ https://www.swift.ac.uk/xrt_products/index.php

⁵ https://swift.gsfc.nasa.gov/archive/grb_table.html/

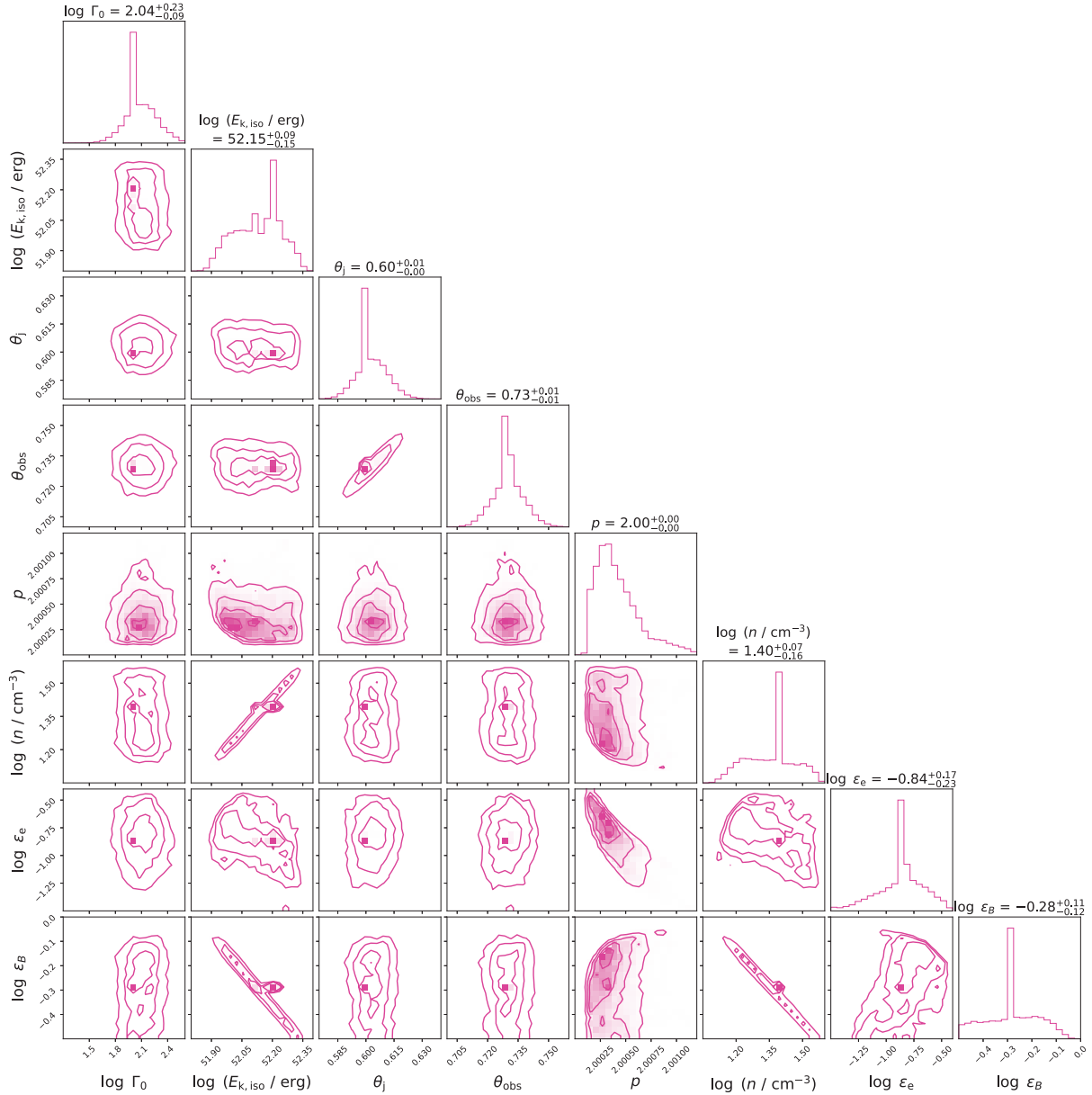


Figure 7. Physical parameters derived by using a top-hat jet model ($1\sigma - 3\sigma$ confidence levels) for GRB 171205A. The best fitting results are marked with 1σ uncertainties above the panel of their posterior distributions.

$\beta_h < -1$. It is worth noting that some selection effects including the instrumental threshold and the galaxy identification as emphasized by Zhang et al. (2018b) have been neglected in the work.

The offsets of GRBs in their host galaxies can help reveal the populations of unusual GRB progenitors (Bloom et al. 2002). Dainotti et al. (2020) reported 22 SN/GRBs and 8 KN/GRBs. Jin et al. (2021) provided another sample including 9 KN/GRBs. Here, we choose these SN/KN-associated GRBs with projected physical offset (R_{phys}) or angular offset (R_{ang}) available to examine their similarity in depth. In total, we have

a sample consisting of 12 SN/GRBs and 10 KN/GRBs. Table 2 lists the key parameters of these SN/GRBs and KN/GRBs and relevant references. The overall distribution of offsets can provide a robust clue to the nature of the progenitors (Bloom et al. 2002). Zhang et al. (2017) have checked the possible correlations between the luminosities of short GRBs with/without extended emission and their offsets to examine the underlying physical origins. Here, similar studies are made to diagnose the possible difference of underlying physical origins between SN/GRBs and KN/GRBs. Figure 5 illustrates their one-dimensional and two-dimensional

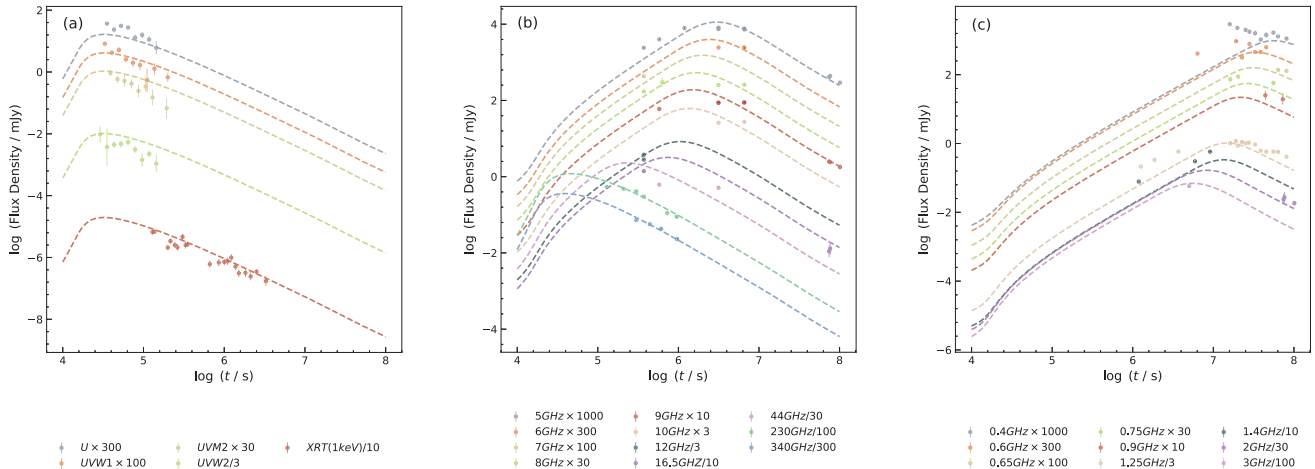


Figure 8. Observed multi-wavelength afterglow of GRB 171205A and the best fitting lightcurves predicted by a top-hat jet model (dashed curves). The data of Swift/XRT/UVOT afterglow light curves in panel (a) are taken from D’Elia et al. (2018). The radio afterglow data in panels (b) and (c) are obtained from Maity & Chandra (2021) and Leung et al. (2021).

distributions on the $L_{\gamma,P} - R_{\text{phys}}$ plane. We see that the offsets of SN/GRBs tend to be smaller than those of KN/GRBs. This result is consistent with the fact that SGRBs typically have a larger offset than that of LGRBs (e.g. Fong et al. 2010; Fong & Berger 2013).

We have performed the Kolmogorov-Smirnov (K-S) test to analyze the difference between the two distributions of KN/GRBs and SN/GRBs. In panel (a), we get $D = 0.64$ from the K-S test, with a p-value of 0.01. Adopting the critical value of $D_{\alpha} = 0.74$ at a significance level of $\alpha = 0.005$, we conclude that the distribution of SN/GRBs is different from that of KN/GRBs. It is further noticed that four LLGRBs, i.e. GRBs 171205A, 170817A, 060218, and 980425, are generally located in the lower section and obviously deviate from the other GRBs due to their very low luminosities. Additionally, we find that there is a moderate correlation between the isotropic prompt luminosity and the offset, with the Pearson correlation coefficient being $\rho = -0.44$ (-0.30) and a chance probability of $P = 0.23$ (0.43) for SN/GRBs (KN/GRBs) after excluding the four LLGRBs. It is similar to the result of Zhang et al. (2017). Since the offset distributions of SN/GRBs and KN/GRBs with longer and shorter durations, are obviously distinct as illustrated by Troja et al. (2008), their luminosities should be related with offsets. However, due to the limited number of LLGRBs, no general conclusion on the correlation between luminosity and offset can be drawn currently.

3.5. Modelling multi-wavelength afterglows

We adopt an overall dynamic evolution and radiation process of jetted GRB ejecta model (Huang et al. 1999, 2000, 2006) to fit the multi-wavelength afterglow of GRB 171205A on condition that a simple top-hat jet model is assumed. We use the Markov Chain Monte Carlo (MCMC) algorithm to get the best fitting result for the multi-wavelength GRB afterglow. The corresponding corner plot of some typical parameters is shown in Figure 7 and Table 3, in which the jet half-opening angle and the viewing angle are found to be ~ 34.4 and 41.8 degrees, respectively, confirming that GRB 171205A was viewed off-axis (see e.g. Maity & Chandra 2021; Kumar et al. 2022). Consequently, the large θ_j should correspond to the angular size of a cocoon rather than the jet core (Li et al. 2020; Maity & Chandra 2021). In addition, we present the observed data of multi-wavelength afterglows and the best fitting light curves in Figure 8.

The Karl G. Jansky Very Large Array Sky Survey (VLASS) revealed that the spectral luminosity of GRB 171205A lies between normal long GRBs and SNe with H-poor prompt spectrum (Stroh et al. 2021). In addition, Arabsalmani et al. (2022) presented a detailed study on the distribution and kinematics of atomic hydrogen in the host galaxy of GRB 171205A through the HI 21cm emission line observation with the JVLA. Its unusual HI features indicate that GRB 171205A could be ignited under extreme conditions with rare dynamics. Here, we find that GRB 171205A is located close to other SN/GRBs in the plane of peak luminosities versus spectral lags, which is consistent with the result of all SN/KN-associated GRBs (Li et al. 2023). The host

Table 2. Physical parameters of the SN/GRBs and KN/GRBs.

GRB	T_{90} (s)	z	offset (R_{phys}) (kpc)	$\log L_{\gamma, \text{p}}$ (erg s $^{-1}$)	Ref.
KN/GRBs					
170817A	2.048	0.009783	2.00±0.02	47.20±0.11	[3][8]
160821B	0.48	0.161	16.40±1.64 ^e	48.94 $^{+0.05}_-0.05$ ^c	[3][10]
150101B	0.012	0.1343	7.30±0.05	48.58 $^{+0.20}_-0.19$ ^c	[3][6]
130603B	0.176	0.3565	5.30±0.20	50.28±0.05	[2][5]
070809	1.28	0.2187	20.00±1.60	49.06±0.04	[2][5]
070714B	3.00	0.9224	12.40±0.90	50.74±0.02	[2][5]
061201	0.76	0.111	32.90±0.10	49.00±0.02	[1][2]
060614	109.104	0.125	1.08±0.04	49.51±0.02	[2][5]
060505	4.0	0.0889	7.16±0.06	48.82 $^{+0.18}_-0.15$ ^c	[3][4]
050709	0.07	0.161	3.80±0.38 ^e	50.73 $^{+0.05}_-0.06$	[3][5][8]
SN/GRBs					
171205A	189.4	0.0368	5.81±0.58 ^{d, e}	47.26±0.09	[2][11]
120422A	5.35	0.28	8.17±0.82 ^e	49.01±0.08	[2][5]
100621A	66.3	0.542	0.28±0.44	50.96±0.02	[2][4]
091127	9.57	0.49	1.34±0.30	51.41±0.02	[2][4]
090618	115.2	0.54	4.40±0.29	51.44±0.01	[2][4]
090424	50.30	0.544	2.59±0.24	51.71±0.03	[2][4]
081007	5.6	0.529	14.44±0.25	50.29±0.05	[2][4]
080319B	147.0	0.937	1.70±0.93	51.73±0.03	[2][4]
060729	120.0	0.54	2.15±0.27	49.91±0.04	[2][4]
060218	2100.0	0.033	0.12±0.03	46.08±0.09	[2][4][12]
050824	38	0.83	3.60±0.41	49.90±0.14	[2][4]
980425	18.0	0.00866	2.34±0.01	47.11±0.02 ^e	[7][9]

Ref. [1] Lü et al. (2015); [2] Dainotti et al. (2020); [3] Jin et al. (2021); [4] Blanchard et al. (2016); [5] Li et al. (2016); [6] Fong et al. (2016); [7] Bloom et al. (2002); [8] Wang et al. (2018); [9] Norris et al. (2000); [10] Zhang et al. (2021); [11] D’Elia et al. (2018); [12] Campana et al. (2006);

^c Calculated as $L_{\gamma, \text{p}} = 4\pi D_L^2 P_{\gamma, \text{bolo}}$.

^d A projected angular offset of $R_{\text{ang}} = 8$ arcsec is reported by D’Elia et al. (2018). We calculate the projected physical offset as $R_{\text{phys}} = D_L / (1+z)^2 R_{\text{ang}}$ (Bloom et al. 2002).

^e Taking 10% of the measured parameter as the error estimation.

Table 3. The best-fit results of GRB 171205A for a Top-hat jet model.

$\log \Gamma$	$\log(E_{\text{k, iso}}/\text{erg})$	θ_j	θ_{obs}	p	$\log(n/\text{cm}^3)$	$\log \epsilon_e$	$\log \epsilon_B$
2.04 $^{+0.22}_-0.09$	52.15 $^{+0.09}_-0.15$	0.60 $^{+0.01}_-0.01$	0.73 $^{+0.01}_-0.01$	2.00 $^{+0.00}_-0.00$	1.40 $^{+0.07}_-0.16$	-0.84 $^{+0.17}_-0.23$	-0.28 $^{+0.11}_-0.12$

galaxy spectrum of GRB 171205A, like other nearby LL-GRBs, has a spectral index lower than -1. Meanwhile, we notice in the plot of $L_{\gamma, \text{iso}}$ against R_{phys} that GRB 171205A is located between SN/GRBs and KN/GRBs. However, the result is somewhat ambiguous owing to a limited number of KN/GRBs with measured offsets.

4. DISCUSSION

The central engine of GRBs may be a magnetar, especially those GRBs with a plateau component in the X-ray afterglow (Xu & Huang 2012; Tang et al.

2019). The total rotational energy of a millisecond magnetar can be written as $E_{\text{rot}} = I\Omega_0^2/2 \simeq 2 \times 10^{52} \text{erg} M_{1.4} R_6^2 P_{0,-3}^{-2}$, where I is the moment of inertia, $P_0 = 2\pi/\Omega_0$ is the initial spin period. M and R are the mass and radius of the NS. The magnetar spins down due to magnetic dipole radiation, and the spin-down luminosity evolves with time as $L_{\text{EM}}(t) = L_{\text{em},0} (1+t/\tau_{\text{c,em}})^{-2}$, where $L_{\text{em},0} \simeq 1.0 \times 10^{49} B_{\text{p},15}^2 P_{0,-3}^4 R_6^6 \text{erg s}^{-1}$ is the initial kinetic luminosity and $\tau_{\text{c,em}} \simeq 2.05 \times 10^3 \text{s} I_{45} B_{\text{p},15}^{-2} P_{0,-3}^2 R_6^{-6}$ is the characteristic spin-down time scale (Lü et al. 2015,

2018). To diagnose the center engine of GRB 171205A, we use the Swift X-ray data to constrain the initial spin period and the dipolar surface magnetic field to test whether the results match the spin-up line predictions for typical neutron star (Stratta et al. 2018). In this way, we constrain the initial spin period as $P_0 \sim (117.6 \pm 0.4)$ ms, with the dipolar surface magnetic field being $B_p \sim (3.73 \pm 0.33) \times 10^{15}$ G. The magnetic field deviates from the bounding of the B_p - P_0 parameters corresponding to the range of mass accretion rates $10^{-4} M_\odot s^{-1} < \dot{M} < 0.1 M_\odot s^{-1}$ (Stratta et al. 2018). Note that $M = 1.35 M_\odot$ and $R = 11.9$ km (Deibel et al. 2013; Lattimer & Prakash 2016; Most et al. 2018) have been adopted in our calculations.

In contrast to those normal GRBs produced from an ultra-relativistic jet driven by a compact central engine, low-luminosity GRBs may be powered by shock breakouts (e.g. Kulkarni et al. 1998; Nakar & Sari 2012). For example, Starling et al. (2012) argued that two low-luminosity GRBs (060218 and 100316D) with thermal spectrum and emitting radius much smaller than those of the normal energetic GRBs can be interpreted by the shock breakout model. However, GRB 171205A as a typical low-luminosity burst has a thermal spectral component but with a temperature close to that of the thermal component in an energetic SN/GRB 101219B (D’Elia et al. 2018). This hints that both low- and high-luminosity SN/GRBs may have the thermal spectrum universally.

Izzo et al. (2019) studied the multi-epoch spectrum of GRB171205A/SN2017iuk and argued that the high speed emission features should originate from a mildly relativistic hot cocoon generated due to the breakout of an ultra-relativistic jet (see also Suzuki & Maeda 2022). The geometric feature of outflow is quite similar to that of the KN/GRB 170817A on basis of multiple-facility radio observations (Mooley et al. 2018a,b). Interestingly, we found that the special structure of a relativistic jet surrounded by a non-relativistic cocoon of GRB 170817A-like events can also be distinguished by the temporal evolution of prompt γ -ray light curves (Li et al. 2020). Subsequently, Maity & Chandra (2021) utilized the upgraded Giant Metre-wave Radio Telescope (uGMRT) to monitor the late radio afterglow (~ 1000 days after burst) of GRB 171205A in a frequency range of 250–1450 MHz and further inferred GRB 171205A to originate from an off-axis jet enveloped by a wide cocoon. Kumar et al. (2022) used the latest XRT data to constrain the jet half-opening angle to be $\theta_j > 51.3$ degrees. For such a large jet half-opening angle, the X-ray afterglow under off-axis condition is expected to peak dozens (or even hundreds) of days af-

ter the GRB detection and the X-ray flux would be very low. However, its X-ray afterglow peaks within ~ 1 day, which resembles other GRB X-ray light-curves viewed on-axis.

In general, GRBs can be physically classified as short-hard (type I) and long-soft (type II) groups according to the multiple classification standards (Zhang et al. 2009). The types I and II bursts are respectively produced by the compact star merger and core-collapse processes. We notice from Li et al. (2023) that almost all SN/GRBs (except GRB 200826A) have durations longer than 2s while most KN/GRBs are short ones with $T_{90} < 2$ s. There are four long KN/GRBs (050724, 060614A, 070714B and 080503) challenging the traditional classification scheme on basis of durations (Kouveliotou et al. 1993; Zhang et al. 2008). This means that a fraction of long GRBs should originate from compact binary collisions instead of core-collapse processes. For example, a recent striking long GRB 211211A associated with kilonova provides a compelling evidence of a compact binary merger origin (e.g. Yang et al. 2022; Troja et al. 2022). On the other hand, Li et al. (2023) systematically compared the temporal and spectral properties of 53 SN/GRBs and 15 KN/GRBs and found a heavy overlap in the plots of luminosity-lag, Amati relation and plateau duration-luminosity between both types of GRBs. In practice, most GRBs do not have an SN or KN detected, but they still could be SN/GRBs or KN/GRBs. In these cases, the SN or KN signals are not detectable because either the signals are too faint or they are buried beneath the brighter GRB afterglow. As a nearby SN/GRB, GRB 171205A exhibits both differences and similarities with normal LGRBs, nearby LLGRBs and SGRBs, indicating that the SN/LLGRB populations might be more complex than what we thought before. Hopefully, our statistical results can shed new light on the nature of GRB 171205A and provide some useful clues for further investigations in the field.

5. CONCLUSIONS

We find that the pulse width and energy of GRB 171205A have a power-law relation with an index of -0.24 ± 0.07 , which is on average larger than those of normal long GRBs. The early X-rays and gamma-rays may reflect the activities of the central engine, while the late X-rays should be resulted from the interaction of the external shock with the circumburst material. Using the 9 SN/GRBs with measured offset, we found that $L_{\gamma,p} \propto \tau^{-1.91}$, which is different from $L_{\gamma,p} \propto \tau^{-1.15}$ derived by Norris et al. (2000) for normal long GRBs. The MCMC method is engaged to fit the multi-wavelength afterglow of GRB 171205A. The jet half-opening angle

and the viewing angle are found to be ~ 34.4 and 41.8 degrees, respectively, confirming the off-axis geometry of this event.

ACKNOWLEDGEMENTS

We thank the anonymous referee for very constructive comments and suggestions that led to an overall improvement of this study. This work was supported by the National Natural Science Foundation of China (No. U2031118), the Youth Innovations and Talents Project

of Shandong Provincial Colleges and Universities (Grant No. 201909118) and the Natural Science Foundations (ZR2018MA030, ZR2023MA049, XKJJC201901). YFH is supported by the National Key R&D Program of China (2021YFA0718500), by National SKA Program of China (No. 2020SKA0120300), and by the National Natural Science Foundation of China (Grant Nos. 12233002, 12041306). YFH also acknowledges the support from the Xinjiang Tianchi Program.

REFERENCES

- Arabsamani M., Roychowdhury S., Renaud F., Burkert A., Emsellem E., Le Floch E., Pian E., 2022, *AJ*, 164, 69. doi:10.3847/1538-3881/ac77f5
- Arimoto M., Kawai N., Asano K., Hurley K., Suzuki M., Nakagawa Y. E., Shimokawabe T., et al., 2010, *PASJ*, 62, 487. doi:10.1093/pasj/62.2.487
- Band, D. L. 1997, *ApJ*, 486, 928. doi:10.1086/304566
- Bennett, C. L., Larson, D., Weiland, J. L., et al. 2014, *ApJ*, 794, 135
- Bernardini M. G., Ghirlanda G., Campana S., Covino S., Salvaterra R., Atteia J.-L., Burlon D., et al., 2015, *MNRAS*, 446, 1129. doi:10.1093/mnras/stu2153
- Beniamini P., Duque R., Daigne F., Mochkovitch R., 2020, *MNRAS*, 492, 2847. doi:10.1093/mnras/staa070
- Blanchard, P. K., Berger, E., & Fong, W.-. 2016, *ApJ*, 817, 144. doi:10.3847/0004-637X/817/2/144
- Bloom, J. S., Kulkarni, S. R., & Djorgovski, S. G. 2002, *AJ*, 123, 1111. doi:10.1086/338893
- Butler, N., Watson, A. M., Kutuyev, A., et al. 2017, GRB Coordinates Network, Circular Service, No. 22182, #1 (2017), 22182
- Bromberg, O., Nakar, E., & Piran, T. 2011, *ApJL*, 739, L55. doi:10.1088/2041-8205/739/2/L55
- Campana, S., Mangano, V., Blustin, A. J., et al. 2006, *nature*, 442, 1008. doi:10.1038/nature04892
- Cano, Z., Wang, S.-Q., Dai, Z.-G., et al. 2017, *Advances in Astronomy*, 2017, 8929054. doi:10.1155/2017/8929054
- Chandra, P., Nayana, A. J., Bhattacharya, D., et al. 2017a, GRB Coordinates Network, Circular Service, No. 22264, #1 (2017), 22264
- Chandra, P., Nayana, A. J., Bhattacharya, D., et al. 2017b, GRB Coordinates Network, Circular Service, No. 22222, #1 (2017), 22222
- Chandra, P. & Frail, D. A. 2012, *ApJ*, 746, 156. doi:10.1088/0004-637X/746/2/156
- Choi, C., Im, M., Gak, L. S., et al. 2017, GRB Coordinates Network, Circular Service, No. 22188, 1 (2017), 22188
- Cobb, B. E. 2017, GRB Coordinates Network, Circular Service, No. 22192, 1 (2017), 22192
- Condon J. J., 1992, *ARA&A*, 30, 575. doi:10.1146/annurev.aa.30.090192.003043
- D’Elia, V., D’Ai, A., Lien, A. Y., et al. 2017, GRB Coordinates Network, Circular Service, No. 22177, #1 (2017), 22177
- D’Elia, V., Campana, S., D’Ai, A., et al. 2018, *A&A*, 619, A66. doi:10.1051/0004-6361/201833847
- Dainotti, M. G., Lenart, A. L., Sarracino, G., et al. 2020, *ApJ*, 904, 97. doi:10.3847/1538-4357/abbe8a
- Deibel, A. T., Steiner, A. W., & Brown, E. F. 2013, *AAS/High Energy Astrophysics Division 13*, 103.08
- Du, X. Y., Zhen, H. Y., Liu, J. X., Zhang, Z. B., Dong, X. F., et al., 2023, *ApJ*, accepted.
- Fan Y.-Z., Xu D., 2006, *MNRAS*, 372, L19. doi:10.1111/j.1745-3933.2006.00217.x
- Fenimore, E. E., in ’t Zand, J. J. M., Norris, J. P., et al. 1995, *ApJL*, 448, L101. doi:10.1086/309603
- Fong, W., Berger, E., & Fox, D. B. 2010, *ApJ*, 708, 9. doi:10.1088/0004-637X/708/1/9
- Fong, W. & Berger, E. 2013, *ApJ*, 776, 18. doi:10.1088/0004-637X/776/1/18
- Fong, W., Margutti, R., Chornock, R., et al. 2016, *ApJ*, 833, 151. doi:10.3847/1538-4357/833/2/151
- Galama, T. J., Vreeswijk, P. M., van Paradijs, J., et al. 1998, *nature*, 395, 670. doi:10.1038/27150
- Gao H., Lei W.-H., Zou Y.-C., Wu X.-F., Zhang B., 2013, *NewAR*, 57, 141. doi:10.1016/j.newar.2013.10.001
- Gao, H., Ren, A.-B., Lei, W.-H., et al. 2017, *ApJ*, 845, 51. doi:10.3847/1538-4357/aa7e30
- Gehrels N., Norris J. P., Barthelmy S. D., Granot J., Kaneko Y., Kouveliotou C., Markwardt C. B., et al., 2006, *Natur*, 444, 1044. doi:10.1038/nature05376
- Granot, J. & Kumar, P., 2006, *MNRAS*, 366, L13. doi:10.1111/j.1745-3933.2005.00121.x

- Hakkila J., Giblin T. W., Norris J. P., Fragile P. C., Bonnell J. T., 2008, *ApJL*, 677, L81. doi:10.1086/588094
- Huang, Y. F., Dai, Z. G., Lu, T. 1999, *MNRAS*, 309, 513. doi:10.1046/j.1365-8711.1999.02887.x
- Huang, Y. F., Gou, L. J., Dai, Z. G., Lu, T. 2000, *ApJ*, 543, 90. doi:10.1086/317076
- Huang, Y. F., Cheng, K. S., & Gao, T. T. 2006, *ApJ*, 637, 873. doi:10.1086/498423
- Huppenkothen, D., Bachetti, M., Stevens, A. L., et al. 2019a, *ApJ*, 881, 39. doi:10.3847/1538-4357/ab258d
- Huppenkothen, D., Bachetti, M., Stevens, A., et al. 2019b, *The Journal of Open Source Software*, 4, 1393. doi:10.21105/joss.01393
- Izzo, L., Selsing, J., Japelj, J., et al. 2017, *GRB Coordinates Network, Circular Service, No. 22180, #1 (2017)*, 22180
- Izzo, L., de Ugarte Postigo, A., Maeda, K., et al. 2019, *nature*, 565, 324. doi:10.1038/s41586-018-0826-3
- Jin, Z.-P., Zhou, H., Covino, S., et al. 2021, arXiv:2109.07694
- Kennea, J. A., Sbarufatti, B., Burrows, D. N., et al. 2017, *GRB Coordinates Network, Circular Service, No. 22183, #1 (2017)*, 22183
- Kisaka, S., Ioka, K., & Sakamoto, T. 2017, *ApJ*, 846, 142. doi:10.3847/1538-4357/aa8775
- Kisaka, S. & Ioka, K. 2015, *ApJL*, 804, L16. doi:10.1088/2041-8205/804/1/L16
- Kouveliotou C., Meegan C. A., Fishman G. J., Bhat N. P., Briggs M. S., Koshut T. M., Paciesas W. S., Pendleton G. N., 1993, *ApJL*, 413, L101
- Kulkarni, S. R., Frail, D. A., Wieringa, M. H., et al. 1998, *nature*, 395, 663. doi:10.1038/27139
- Kumar, P. & Zhang, B. 2015, *PhR*, 561, 1. doi:10.1016/j.physrep.2014.09.008
- Kumar A., Pandey S. B., Gupta R., Aryan A., Ror A. K., Sharma S., Brahme N., 2022, *NewA*, 97, 101889. doi:10.1016/j.newast.2022.101889
- Lattimer J. M., Prakash M., 2016, *PhR*, 621, 127. doi:10.1016/j.physrep.2015.12.005
- Leung, J. K., Murphy, T., Ghirlanda, G., et al. 2021, *MNRAS*, 503, 1847. doi:10.1093/mnras/stab326
- Liang, E.-W., Zhang, B.-B., Stamatikos, M., et al. 2006, *ApJL*, 653, L81. doi:10.1086/510516
- Li, L.-B., Zhang, Z.-B., Huang, Y.-F., et al. 2015, *MNRAS*, 451, 1815. doi:10.1093/mnras/stv985
- Li, Q. M., Zhang, Z. B., Han, X. L., et al. 2023, *MNRAS*, 524, 1096. doi:10.1093/mnras/stad1648
- Li, X. J., Zhang, Z. B., Zhang, X. L., et al. 2021a, *ApJS*, 252, 16. doi:10.3847/1538-4365/abd3fd
- Li, X. J., Zhang, Z. B., & Zhang, K. 2022a, *A&A*, 657, A124. doi:10.1051/0004-6361/202140747
- Li, X.-J., Zhang, Z.-B., Zhang, C.-T., et al. 2020, *ApJ*, 892, 113. doi:10.3847/1538-4357/ab7a94
- Li, Y., Zhang, B., & Lü, H.-J. 2016, *ApJS*, 227, 7. doi:10.3847/0067-0049/227/1/7
- Lien, A., Sakamoto, T., Barthelmy, S. D., et al. 2016, *ApJ*, 829, 7. doi:10.3847/0004-637X/829/1/7
- Lipunov, V., Gorbovskey, E., Kornilov, V., et al. 2017, *GRB Coordinates Network, Circular Service, No. 22226, 1 (2017)*, 22226
- Lü, H.-J., Zhang, B., Lei, W.-H., et al. 2015, *ApJ*, 805, 89. doi:10.1088/0004-637X/805/2/89
- Lü, H.-J., Zou, L., Lan, L., et al. 2018, *MNRAS*, 480, 4402. doi:10.1093/mnras/sty2176
- Lü, H.-J., Yuan, Y., Lan, L., et al. 2020, *ApJL*, 898, L6. doi:10.3847/2041-8213/aba1ed
- Maity, B. & Chandra, P. 2021, *ApJ*, 907, 60. doi:10.3847/1538-4357/abd2be
- Makhathini, S., Mooley, K. P., Brightman, M., et al. 2021, *ApJ*, 922, 154. doi:10.3847/1538-4357/ac1ffc
- Malesani, D., Tagliaferri, G., Chincarini, G., et al. 2004, *ApJL*, 609, L5. doi:10.1086/422684
- Mészáros, P. & Rees, M. J. 1997, *ApJ*, 476, 232. doi:10.1086/303625
- Mooley, K. P., Nakar, E., Hotokezaka, K. et al., 2018, *Nature*, 554, 207. doi:10.1038/nature25452
- Mooley, K. P., Deller, A. T., Gottlieb, O. et al., 2018, *Nature*, 561, 355, doi:10.1038/s41586-018-0486-3
- Most E. R., Weih L. R., Rezzolla L., Schaffner-Bielich J., 2018, *PhRvL*, 120, 261103. doi:10.1103/PhysRevLett.120.261103
- Nousek, J. A., Kouveliotou, C., Grupe, D., et al., 2006, *ApJ*, 642, 389. doi:10.1086/500724
- Norris, J. P., Nemiroff, R. J., Bonnell, J. T., et al. 1996, *ApJ*, 459, 393. doi:10.1086/176902
- Norris, J. P., Marani, G. F., & Bonnell, J. T. 2000, *ApJ*, 534, 248. doi:10.1086/308725
- Norris J. P., 2002, *ApJ*, 579, 386. doi:10.1086/342747
- Norris, J. P. & Bonnell, J. T. 2006, *ApJ*, 643, 266. doi:10.1086/502796
- Norris, J. P., Gehrels, N., & Scargle, J. D. 2011, *ApJ*, 735, 23. doi:10.1088/0004-637X/735/1/23
- Nakar, E. & Sari, R. 2012, *ApJ*, 747, 88. doi:10.1088/0004-637X/747/2/88
- Paczyński, B. 1998, *ApJL*, 494, L45. doi:10.1086/311148
- Pian, E., Mazzali, P. A., Masetti, N., et al. 2006, *nature*, 442, 1011. doi:10.1038/nature05082
- Popham, R., Woosley, S. E., & Fryer, C. 1999, *ApJ*, 518, 356. doi:10.1086/307259
- Rees, M. J. & Meszaros, P. 1994, *ApJL*, 430, L93. doi:10.1086/187446

- Rosswog, S. 2007, MNRAS, 376, L48.
doi:10.1111/j.1745-3933.2007.00284.x
- Rowlinson, A., O'Brien, P. T., Metzger, B. D., et al. 2013, MNRAS, 430, 1061. doi:10.1093/mnras/sts683
- Rybicki, G. B. & Lightman, A. P. 1979, A Wiley-Interscience Publication, New York: Wiley, 1979
- Sari, R. 1997, ApJL, 489, L37. doi:10.1086/310957
- Schaefer B. E., Collazzi A. C., 2007, ApJL, 656, L53.
doi:10.1086/512855
- Sharma, V., Iyyani, S., & Bhattacharya, D. 2021, ApJL, 908, L2. doi:10.3847/2041-8213/abd53f
- Soderberg, A. M., Berger, E., Kasliwal, M. et al., 2006, ApJ, 650, 271. doi:10.1086/506429
- Starling, R. L. C., Wiersema, K., Levan, A. J., et al. 2011, MNRAS, 411, 2792. doi:10.1111/j.1365-2966.2010.17879.x
- Starling, R. L. C., Page, K. L., Pe'Er, A., et al. 2012, MNRAS, 427, 2950. doi:10.1111/j.1365-2966.2012.22116.x
- Stratta, G., Dainotti, M. G., Dall'Osso, S., et al. 2018, ApJ, 869, 155. doi:10.3847/1538-4357/aadd8f
- Stroh, M. C., Terreran, G., Coppejans, D. L. et al., 2021, ApJL, 923, L24. doi:10.3847/2041-8213/ac375e
- Suzuki, A., Maeda, K., 2022, ApJ, 925, 148.
doi:10.3847/1538-4357/ac3d8d
- Troja, E., King, A. R., O'brien, P. T., et al. 2008, MNRAS, 385, L10. doi:10.1111/j.1745-3933.2007.00421.x
- Troja, E., Fryer, C. L., O'Connor, B., et al. 2022, Nature, 612, 228. doi:10.1038/s41586-022-05327-3
- Tang, C.-H., Huang, Y.-F., Geng, J.-J., Zhang, Z.-B. 2019, ApJS, 245, 1. doi:10.3847/1538-4365/ab4711
- Tatarnikov, A. 2018, The Astronomer's Telegram, 11514
- Terreran, G., Fong, W., Margutti, R., et al. 2019, GRB Coordinates Network, Circular Service, No. 25664, 25664
- Trushkin, S. A., Erkenov, A. K., Tsybulev, P. G., et al. 2017, GRB Coordinates Network, Circular Service, No. 22258, 22258
- Uhm, Z. L., Zhang, B., & Racusin, J. 2018, ApJ, 869, 100.
doi:10.3847/1538-4357/aaeb30
- Ukwatta T. N., Stamatikos M., Dhuga K. S., Sakamoto T., Barthelmy S. D., Eskandarian A., Gehrels N., et al., 2010, ApJ, 711, 1073. doi:10.1088/0004-637X/711/2/1073
- Ukwatta T. N., Dhuga K. S., Stamatikos M., Dermer C. D., Sakamoto T., Sonbas E., Parke W. C., et al., 2012, MNRAS, 419, 614. doi:10.1111/j.1365-2966.2011.19723.x
- Urata, Y., Toma, K., Huang, K., et al. 2019, ApJL, 884, L58. doi:10.3847/2041-8213/ab48f3
- Usov, V. V. 1992, nature, 357, 472. doi:10.1038/357472a0
- Valan, V. & Larsson, J. 2021, MNRAS, 501, 4974.
doi:10.1093/mnras/staa3978
- Wang, J., Zhu, Z. P., Xu, D., et al. 2018, ApJ, 867, 147.
doi:10.3847/1538-4357/aae6c3
- Wang, Y., Becerra, L. M., Fryer, C. L., et al. 2023, ApJ, 945, 95. doi:10.3847/1538-4357/acb771
- Wei, J.-J., Zhang, B.-B., Shao, L., et al. 2017, ApJL, 834, L13. doi:10.3847/2041-8213/834/2/L13
- Woosley, S. E. & Heger, A. 2006, ApJ, 637, 914.
doi:10.1086/498500
- Xu, F., Tang, C.-H., Geng, J.-J., et al. 2021, ApJ, 920, 135.
doi:10.3847/1538-4357/ac158a
- Xu, F., Huang, Y. F., Geng, J.-J., et al. 2022, A&A, in revision.
- Xu, M. & Huang, Y.F. 2012, A&A, 538, A134.
doi:10.1051/0004-6361/201117754
- Yang, J., Ai, S., Zhang, B.-B., et al. 2022, Nature, 612, 232.
doi:10.1038/s41586-022-05403-8
- Yu Y. B., Wu X. F., Huang Y. F., Coward D. M., Stratta G., Gendre B., Howell E. J., 2015, MNRAS, 446, 3642.
doi:10.1093/mnras/stu2336
- Yin, Q. & Hou, S. 2021, 43rd COSPAR Scientific Assembly. Held 28 January - 4 February, 43, 1643p.1643
- Zhang B., Mészáros P., 2001, ApJL, 552, L35.
doi:10.1086/320255
- Zhang B., Mészáros P., 2004, International Journal of Modern Physics A, 19, 2385. doi: 10.1142/S0217751X0401746X
- Zhang, B., Fan, Y. Z., Dyks, J., et al., 2006, ApJ, 642, 354.
doi:10.1086/500723
- Zhang, B., 2007, Chinese Journal of Astronomy and Astrophysics, 7, 1. doi:10.1088/1009-9271/7/1/01
- Zhang, B., Zhang, B.-B., Virgili, F. J., et al. 2009, ApJ, 703, 1696. doi:10.1088/0004-637X/703/2/1696
- Zhang, B. 2018, The Physics of Gamma-Ray Bursts by Bing Zhang. ISBN: 978-1-139-22653-0. Cambridge Univeristy Press, 2018. doi:10.1017/9781139226530
- Zhang, B. T., Murase, K., Yuan, C., et al. 2021, ApJL, 908, L36. doi:10.3847/2041-8213/abe0b0
- Zhang, F.-W. 2008, ApJ, 685, 1052. doi:10.1086/590951
- Zhang, S., Jin, Z.-P., Zhang, F.-W., et al. 2017, ApJ, 844, 55. doi:10.3847/1538-4357/aa7aa7
- Zhang, X.-L., Zhang, C.-T., Li, X.-J., et al. 2020, Research in Astronomy and Astrophysics, 20, 201.
doi:10.1088/1674-4527/20/12/201
- Zhang, X. L., Zhang, Z. B., Li, D., et al. 2023, submitted to MNRAS.
- Zhang, Z.-B., Deng, J.-G., Lu, R.-J., et al. 2006a, ChJA&A, 6, 312. doi:10.1088/1009-9271/6/3/06
- Zhang, Z. B., Xie, G. Z., Deng, J. G., et al., 2006b, MNRAS, 373, 729. doi:10.1111/j.1365-2966.2006.11058.x
- Zhang, Z. B., Xie, G. Z., Choi, C. S., 2008, IJMPD, 17, 1391. doi: 10.1142/S0218271808012966

Zhang Z. B., Choi C. S., 2008, *A&A*, 484, 293. doi:
10.1051/0004-6361:20079210

Zhang, Z. B., Zhang, C. T., Zhao, Y. X., et al. 2018a,
PASP, 130, 054202. doi:10.1088/1538-3873/aaa6af

Zhang, Z. B., Chandra, P., Huang, Y. F., Li, D. 2018b,
ApJ, 865, 82. doi:10.3847/1538-4357/aadc62

Zou, Y.-C., Wang, F.-F., Moharana, R., et al. 2018, *ApJL*,
852, L1. doi:10.3847/2041-8213/aaa123